

# Texture Descriptors and Machine Learning Algorithms for Mistletoe Detection in Urban Forests Using Multispectral Imagery

Paola Andrea Mejia-Zuluaga<sup>a</sup>, Juan C. Valdiviezo-N<sup>b</sup>, and León Dozal<sup>c\*</sup>

<sup>a</sup>Centro de Investigación en Ciencias de Información Geoespacial (CentroGeo), Ciudad de México 14240, Mexico

<sup>b</sup>CONAHCYT—CentroGeo, Department of Remote Sensing, Yucatán 97302, Mexico

<sup>c</sup>CONAHCYT—CentroGeo, Department of Remote Sensing, Aguascalientes 20313, Mexico

## ABSTRACT

In this study, we compare the performance of texture descriptors and spectral vegetation indices for the classification of a hemiparasitic plant that grows on host trees, known as mistletoe. For this purpose, we computed 180 image features, including GLCM, Gabor, and LBPs, as well as spectral vegetation indices, from multispectral aerial image sets. Our image feature database is then classified using Support Vector Machines, with optimized hyperparameters, and accuracy metrics are reported in order to evaluate the contribution of specific feature sets for our application. In addition, we make use of feature selection algorithms in order to determine which combination of descriptors improves the classification process. The study has important implications for the remote sensing community, as it can provide insights into the use of texture and spectral descriptors for classification of the mistletoe species known as *Struthanthus Interruptus*. The results of the study can be used to develop more effective tools to monitor the spread of the pest in urban parks, which can help to preserve trees and ensure their long-term health. Overall, the study contributes to the growing body of research on the use of remote sensing technologies, in conjunction with artificial intelligence techniques, to monitor urban environments.

**Keywords:** Forest pest, Genetic algorithms, Mistletoe classification, Texture features, Vegetation indices.

## 1. INTRODUCTION

In recent years, Remote Sensing (RS) has played an important role for forest pest monitoring given the acquisition possibilities of high-resolution images through unmanned aerial vehicles (UAVs).<sup>1</sup> In particular, the autonomous identification of mistletoe species has become of particular interest because of their rapid spreading mechanisms; mistletoe is a hemiparasitic plant that grows on host trees of coniferous and broad-leaved forests, woodlands, and urban parks by inserting a modified root in the first layers of the host's branches. Thus, once the plant is established as an extension of the tree, it can access to salts, minerals, and water, reducing the quality of life of the host.

Some studies have concluded that there exist three main mistletoe species covering parks and urban forests of Mexico City, known as *Phoradendron velutinum*, *Struthanthus Interruptus*, and *Cladocolea loniceraeoides*, respectively.<sup>2</sup> These species present proper anatomic, phenology, and morphology characteristics, whose distribution has been partially identified through field sampling; for instance, *Struthanthus Interruptus* (*S. Interruptus*) is a type of mistletoe commonly found in urban areas of Mexico city. Its leaf structure, color appearance, and distribution around the host tree make it easily confused with other vegetation species. In fact, its visual identification, both from field work or aerial images, represents a challenging task, being necessary to design specific strategies and techniques to support its identification. Since this pest is rapidly expanding through green areas of Mexico City, there is an urgent need to develop technological tools designed to (1) the identification of mistletoe from host trees, (2) the estimation of the infestation degree, and (3) an adequate control and mitigation of the propagation.

---

Further author information: leon.dozal@gmail.com

In the state of the art, there exist a few works addressing the problem of the automatic identification of mistletoe species.<sup>3–5</sup> For instance, a research aimed at the individual delineation of trees infected by mistletoe species, *Viscum album*, from high-resolution UAV color images, is presented in [6]; for this purpose, a set of spectral vegetation indices and a Random Forest classifier were employed. Moreover, an algorithm designed to detect *Phoradendron velutinum* mistletoe from multispectral images, collected over a forest conservation area, is reported in [7]; the algorithm was designed using Genetic Programming, which has shown promising results. On the other hand, previous remote sensing studies have demonstrated that feature descriptors extracted from the collected imagery greatly improve the classification performance.<sup>8,9</sup> For example, for vegetation classification, several studies make use of texture descriptors, spectral indices, and color spaces. However, one of the main problems in this process lies in the adequate selection of the number and the optimal set of features that maximize the differences among classes. Therefore, in order to design a computational tool for classification of *S. Interruptus* species from aerial images, the objectives of this research are the following. First, we investigate the set of features, including textural descriptors and spectral indices, that improve the identification of this mistletoe species with respect to the host tree. Second, we define some optimal set of feature descriptors, based on Genetic Algorithms (GA) and Principal Component Analysis (PCA), to be included in supervised classification schemes. Third, we evaluate the performance of support vector machines (SVM), based on the previously determined image feature sets, for mistletoe classification.

The organization of the manuscript is the following. In Section 2, we first present the main characteristics of the study area, including a brief description of *S. Interruptus* species; then, the image acquisition process and the construction of our image database are detailed; later, the techniques employed for feature extraction are also presented in this section. Section 3 describes several mistletoe classification schemes, based on SVM with optimized parameters; accuracy metrics for each experiment are reported at the end. Section 4 starts with a discussion of the obtained results, and the main conclusions and direction for future work are also stated.

## 2. MATERIALS AND METHODS

### 2.1 Study area

The chosen study site is known as Ramón López Velarde Garden, located in the heart of Mexico City, at coordinates 19.409629° N, -99.156346° W. This park belongs to the Cuauhtémoc Delegation, comprising 7.4 hectares of forested land, where several tree species, such as *Casuarina sp.*, *Eucalyptus sp.*, *Fraxinus sp.*, *Cupressus sp.*, *Ligustrum sp.*, and *Grevillea sp.* find sanctuary;<sup>10</sup> according to statistics given by the Mexico City Environment Secretariat (SEDEMA),<sup>11</sup> in 2016 the green areas were infested with approximately 60% of *Struthanthus Interruptus* mistletoe. Given the high percentage of infestation and the lack of recent studies, this park is considered as an interesting site for data acquisition and experimentation oriented to the autonomous identification of mistletoe. Figure 1 shows the location of the study area.

*S. Interruptus* is a hemiparasitic plant with aerial roots (epicortical roots) that encircles the branches of the host tree. Its leaves are elongated and have a greyish-green hue in the study site. It also contains small spike-shaped flowers and berry-shaped fruits.<sup>12</sup> This mistletoe species covers a significant portion of the woodland in the research site; at early stages, the location of small foci of infestation with the naked eye is difficult because the first branches and leaves blend in with the host trees of the area; however, in more advanced stages of infestation, this species covers the treetops like a woven blanket, making it possible to spot areas of concentration (See Fig. 2). The entities in charge of the environmental sanitation of Mexico City's green spaces usually conduct field trips to control this kind of pest in forests. Hence, the basic control method entails field work to detect and eradicate mistletoe infested regions. It should be emphasized that mistletoe is visually identified by trained experts; nonetheless, its differentiation from the host tree represents a difficult and challenging task, even for those forestry experts.

### 2.2 Image Database

Aerial images were acquired using a P4 multispectral Unmanned Aerial Vehicle over the study area on September 22, 2022; onboard sensors are capable of collecting five spectral images covering the visible to near-infrared ranges of the electromagnetic spectrum, according to the following band designations and corresponding wavelength intervals:  $R = 450 \text{ nm} \pm 16 \text{ nm}$ ,  $G = 560 \text{ nm} \pm 16 \text{ nm}$ ,  $B = 650 \text{ nm} \pm 16 \text{ nm}$ ,  $REG = 730 \text{ nm} \pm 16 \text{ nm}$ ,

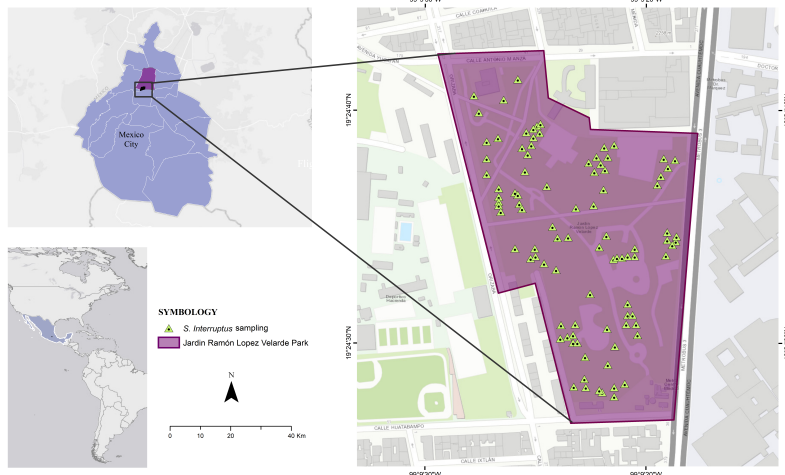


Figure 1: Location of the Ramón López Velarde Garden in Mexico City.

and  $NIR = 840 \text{ nm} \pm 26 \text{ nm}$ , where  $R$ ,  $G$ ,  $B$ ,  $REG$ , and  $NIR$  represent the red, green, blue, red-edge, and near-infrared bands of the collected imagery.

The extension of the study area was covered in 460 image sets in both orthogonal and oblique modes. Table 1 displays some characteristics of the flight plan used to register the images with the UAV. Prior to the analysis, the image collections were co-registered in order to compensate for geometric displacements between the  $REG$  and  $NIR$  bands with respect to the  $R, G, B$  channels, caused by a shutter lag of the corresponding sensors. Another pre-processing step consisted of the photo-interpretation of the images to visually delineate those pixels representing mistletoe regions in order to create reference masks; this process was realized by a trained expert, whose resulting masks were visually corrected and validated by other two members of the project. In a last step, our image database was created by selecting 543 tiles of  $300 \times 300$  pixels, with more than 10% of infestation, from the previous reference masks. Therefore, this set of images was employed for subsequent training and validation of our classification algorithms.



Figure 2: Aerial RGB images of tree species infested by *Struthanthus Interruptus* (encircled in red line) in the study area; (a) oblique image and (b) orthogonal image

Table 1: Flight plan specifications for the P4 multispectral UAV

Parameters	Value
Flight height	70 meters
GSD	3.7 cm/px
Front overlap	70%
Side overlap	30%
Image acquisition mode	Orthogonal and Oblique

### 2.3 Hardware and Software

The experiments presented in this research paper were run on a Server with the following characteristics: Intel(R) Xeon(R) CPU e5-2620 v2, with 2.10 GHz, Ubuntu 14.04 (64-bits) as the operating system, and 24 hyper-threading cores. The co-registration of the image collections was carried out in Matlab(R), while the photo-interpretation of mistletoe was realized with the annotation tool named as CVAT (<https://www.cvat.ai/>). The classification experiments were coded in Python 3.7, using the corresponding libraries.

### 2.4 Image descriptors

In this study, we are interested in the evaluation of image descriptors, extracted from the aerial multispectral sets, with the aim to improve the identification of *S. Interruptus*. For this purpose, we selected both textural and spectral features, including GLCM-based descriptors, Gabor filters, and Local Binary Patterns, as well as spectral indices, which are briefly described in the following lines.

#### 2.4.1 Spectral vegetation indices

Land cover properties may be emphasized by using different wavelength intervals within the electromagnetic spectrum.<sup>13</sup> A simple and effective solution for land cover characterization is based on the algebraic operations among spectral bands of a multispectral set, a technique frequently known as a spectral index (SI). Although spectral indices were designed for particular purposes, their range of applications have increased over time due to their versatility and easy of implementation.

In particular, spectral vegetation indices (VI) have been proposed to analyze physical phenomena related to the distinctive characteristics of plants,<sup>14</sup> including species categorization, water stress, plant density, and health. A good example is the well-known *Normalized Difference Vegetation Index* (NDVI), which was first proposed to monitor the health status of vegetation and has since been discovered to be helpful for crop estimation, as well as droughts and burned regions monitoring.<sup>8,15</sup>

Based on a literature review, a subset of vegetation indices were selected and computed from our multispectral database to support the spectral description of mistletoe *S. Interrumpus*; the selected vegetation indices and their corresponding Equations are displayed in Table 2.

#### 2.4.2 GLCM Features

Texture features in digital images can be measured and segmented by the well known technique proposed by Haralick et al.,<sup>38</sup> known as *the spatial gray-level dependence method*. This method assumes that all the texture information is contained in a gray-level co-occurrence matrix (GLCM), which is used to measure the relations (number of adjacencies) between pixels  $i$  and  $j$ , within a given image; these relations are computed at a given distance ( $d$ ) and specific directions ( $\phi$ ). Then, from the computed GLCM, fourteen texture features were proposed by the authors. For instance, Contrast ( $Con$ ), Dissimilarity ( $Dis$ ), Homogeneity ( $Hom$ ), and Angular Second Moment ( $ASM$ ) are computed according to the following expressions:

$$Con = \sum_i \sum_j (i - j)^2 C_{i,j}, \quad Dis = \sum_i \sum_j |i - j| C_{i,j}. \quad (1)$$

$$Hom = \sum_i \sum_j \frac{1}{1 + (i - j)^2} C_{i,j}, \quad ASM = \sum_i \sum_j C_{i,j}^2. \quad (2)$$

Table 2: Spectral vegetation indices employed for the spectral description of *S. Interrumpus*. Notice that  $R$ ,  $G$ ,  $B$ ,  $REG$ , and  $NIR$  correspond to the red, green, blue, red-edge, and near-infrared bands, respectively.

Vegetation Index	Equation
NDVI (Normalized Difference Vegetation Index) <sup>16</sup>	$(NIR - R)/(NIR + R)$
EVI (Enhanced Vegetation Index) <sup>17</sup>	$2.5 \times [(NIR - R)/(NIR + R - 7.5 \times B + 1)]$
SAVI (Soil Adjusted Vegetation Index) <sup>18</sup>	$[(NIR - R)/(NIR + R + 0.5)] \times (1 + 0.5)$
MSAVI (Modified Soil Adjusted Vegetation Index) <sup>19</sup>	$[2NIR + 1 - \sqrt{(2NIR + 1)^2 - (8NIR - R)}]/2$
ARVI (Atmospherically Resistant Vegetation Index) <sup>20</sup>	$[NIR - (2R - B)]/[NIR + (2R - B)]$
DVI (Difference Vegetation Index) <sup>21</sup>	$NIR - R$
GNDVI (Green Normalized Difference Vegetation Index) <sup>22</sup>	$(NIR - G)/(NIR + G)$
NDRE (Normalized Difference Red Edge) <sup>23</sup>	$(NIR - REG)/(NIR + REG)$
CI (Chlorophyll Index RedEdge) <sup>24</sup>	$(NIR/REG) - 1$
SIPPI (Structure Insensitive Pigment Index) <sup>25</sup>	$(NIR - B)/(NIR - R)$
MTVI (Modified Triangular Vegetation Index) <sup>26, 27</sup>	$1.5 \times (1.2 \times (NIR - G) - 2.5 * (R - G))$
GARI (Green Atmospherically Resistant Index) <sup>28, 29</sup>	$[NIR - G - 1.7(B - R)]/[NIR + G - 1.7(B - R)]$
VARI <sub>G</sub> (Visible Atmosphere Resistant Index Green) <sup>30</sup>	$(G - R)/(G + R - B)$
SR (Simple Ratio) <sup>31</sup>	$NIR/R$
RGRI (Red Green Ratio Index) <sup>32</sup>	$R/G$
BRI (Red Blue Ratio Index) <sup>33</sup>	$R/B$
RDVI (Renormalized Difference Vegetation Index) <sup>34</sup>	$(NIR - R)/\sqrt{NIR + R}$
GLI (Green Leaf Index) <sup>35</sup>	$(2 \times G - R - B)/(2 \times G + R + B)$
MSR (Modified Simple Ratio) <sup>36</sup>	$[(NIR/R) - 1]/\sqrt{[(NIR/R) + 1]}$
PSRI (Plant Senescence Reflectance Index) <sup>37</sup>	$(R - G)/REG$

where  $C_{i,j}$  denotes the gray-level co-occurrence matrix for pixels  $i$  and  $j$ . Based on several experiments on our database, we determined that only five texture features provided with the maximum contrast between mistletoe and the surrounding background. Hence, texture features were computed according to the parameters shown in Table 3; taking into account these parameters combinations, a total number of 60 texture descriptors were computed from every input image.

Table 3: GLCM parameters used for texture descriptors.

Parameters	Value
Texture feature	Con, Dis, Ene, ASM, Hom
Direction	0°, 45°, 90° and 135°
Kernel size	3, 5, 7
Distance	1

#### 2.4.3 Gabor Filters

Gabor filters are composed of a bank of texture descriptors that consider the spatial frequency and orientation of the image, focusing on local characteristics. A sine wave modulated by a Gaussian function conforms a Gabor filter, indicating that the sine wave will have its highest amplitude at the center of the Gaussian function.<sup>39</sup> Mathematically, the Gabor filters are represented by

$$g(x, y; \lambda, \theta, \psi, \sigma, \gamma) = \exp\left(-\frac{x'^2 + \gamma^2 y'^2}{2\sigma^2}\right) \cos\left(2\pi \frac{x'}{\lambda} + \psi\right), \quad (3)$$

where  $x' = x \cos(\theta) + y \sin(\theta)$ ,  $y' = -x \sin(\theta) + y \cos(\theta)$ ,  $\lambda$  is the wavelength of the cosine factor,  $\theta$  is the normal to parallel orientation of the filter fringes,  $\psi$  is the displacement phase,  $\sigma$  is the standard deviation of envelope, and  $\gamma$  is the spatial aspect ratio that specified the ellipticity of the Gaussian hull.

In digital image processing, a Gabor filter is applied through the convolution operation; as a result, particular regions of the image that match the periodicity of the sine wave are emphasized. Thus, depending on how the parameters are changed, it is possible to highlight or suppress particular texture features. The effect of the filter on the texture, orientation, and scale of the image is controlled by parameters. For instance, features of various sizes can be captured depending on the kernel ( $k$ ) size. A large  $\sigma$  value creates a more forgiving and smooth filter, capturing large features, while a smaller value will expose fine details. Similarly, a large  $\lambda$  value will concentrate on larger-scale features and a small one on fine details. Therefore, there exist numerous possible parameter combinations to define an adequate filter bank for an specific application.

In this research, we established some criteria to define a Gabor filter bank oriented to emphasize texture information of the *S. Interruptus* from aerial images. For this purpose, we first created a standard bank filter, conformed by  $k = \{3, 5, 7\}$ ,  $\lambda = \{2, 4, 6\}$ , and  $\sigma = \{1.5, 2, 2.5\}$  values, respectively, all of which take into account the average of four directions  $\theta = \{0^\circ, 45^\circ, 90^\circ, 135^\circ\}$ . Indeed, this filter bank was pre-selected using both a visual examination of the resulting images and a literature review.<sup>40-42</sup> Later, the pre-selected filters were applied to a subset of test images and the Entropy measure ( $H$ ) of the resulting images was computed; we employed the  $H$  measure<sup>43</sup> to determine the amount of texture information that each filter adds in the resulting images. Finally, the filter entropy values were averaged, and those filters satisfying the relation  $H >= \tau$  were selected; notice that  $\tau = \mu + \sigma$  was a threshold value defined to select those filters providing more texture information, with  $\mu$  equals to the mean Entropy value and  $\sigma$  its standard deviation. Table 4 shows the combination of 16 selected Gabor filters, which were applied to every multispectral band of the database to obtain texture descriptors.

Table 4: Parameters of the Gabor filter bank selected for the texture description of *S. Interruptus*.

Kernel ( $k$ )	lambda ( $\lambda$ )	sigma ( $\sigma$ )
3	2	1.5 - 2 - 2.5
5	2	1.5 - 2 - 2.5
5	4	1.5 - 2 - 2.5
7	2	1.5 - 2 - 2.5
7	4	1.5 - 2 - 2.5
7	6	2.5

#### 2.4.4 Local binary patterns

Local binary patterns (LBPs) represent a simple computational method for measuring the spatial structure of image textures; important advantages of this operator are the robustness to gray-scale variations and the rotation-invariant property.<sup>44</sup> The basic LBPs are calculated from a given central pixel  $g_c = g(x, y)$  and its surrounding neighboring pixels,  $g_p = g(x_p, y_p)$ , for  $p = 1, \dots, P$ , on a basis of a radius  $R$  defined from  $g_c$ ; in mathematical form,

$$LBP_{P,R}[g_c] = \sum_{p=0}^P s[g_p - g_c]2^p, \quad (4)$$

where  $x_p = x + R \cos(2\pi \cdot p/P)$ ,  $y_p = y - R \sin(2\pi \cdot p/P)$ , and

$$s(t) = \begin{cases} 1, & \text{if } t \geq 0 \\ 0, & \text{otherwise} \end{cases}$$

For our current application, we established the following LBP parameters for texture description:  $P = \{8, 16, 24\}$  and  $R = \{1, 3\}$ . As with the previous descriptors, these parameters combinations were applied to every multispectral band within the database.

### 3. EXPERIMENTS

The texture and spectral descriptors stated in Section 2.4 were computed for every multispectral band of the selected 543 tiles that comprises our database. With the aim to improve the hardware requirements of our experiments, the multispectral bands together with their corresponding GLCM, Gabor, LBP, and VI images were vectorized independently, as illustrated in Fig. 3; as a result, each column of the vectorized database represents a particular descriptor, while each row represents a pixel position of the image.

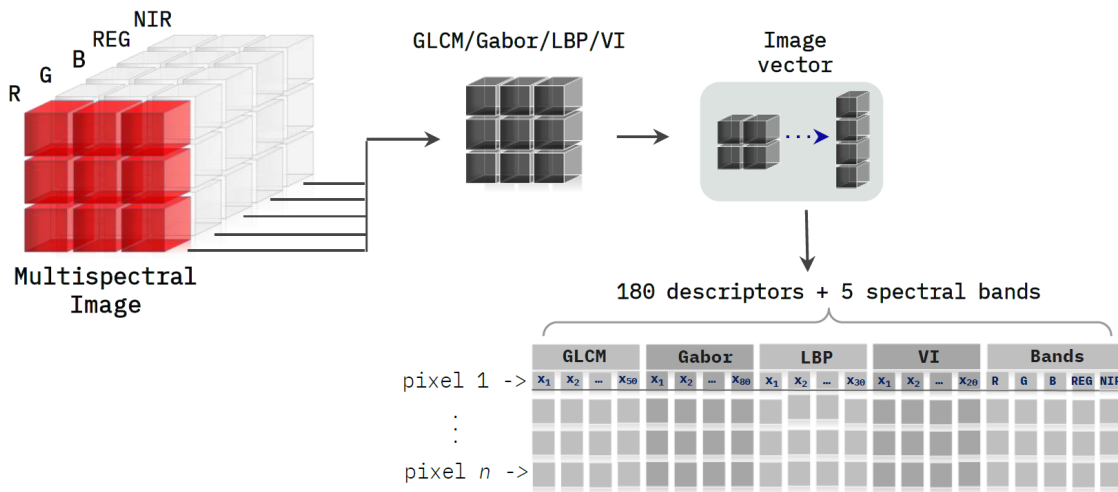


Figure 3: Illustration of the process to create the texture and spectral image database

The experimental design was structured to address two distinct sets of image characteristics. The first set was focused on the examination of full data and is further divided into three categories: analysis based on only spectral bands, analysis based on texture descriptors, and a combined analysis incorporating both spectral bands and texture descriptors. The objective of this experiment was to evaluate the intrinsic utility of such individual sets and the improvements achieved by their combined use for mistletoe classification.

The second set of experiments incorporated feature selection algorithms oriented to improve the classification performance by identifying those relevant characteristics that better describe the *S. Interruptus* species. In this set, two distinct methodologies were employed for feature selection, namely: Principal Component Analysis and Genetic Algorithms.

#### 3.1 Classification results

All experiments were conducted utilizing a random sample of 100,000 pixels taken from the vectorized database, whose information represents the presence and absence of mistletoe across all considered spectral bands and texture descriptors. This database sample was subjected to normalization and standardization processes, achieving a mean of zero and a variance of one. The processed data were then employed to construct the training and validation data sets, which were evaluated within a cross-validation framework using a  $k$ -value of 5.

For the classification process, we employed a Support Vector Machine, with a Radial Base Function (RBF) kernel; the remaining SVM hyperparameters were optimized using the Randomized Search technique,<sup>45</sup> based on three distinct descriptor sets, to obtain the best performance. First, we used the intensity information collected in the five spectral bands of the imagery; in this case, the SVM parameters were set as  $C = 100$  and  $\gamma = 0.100$ .

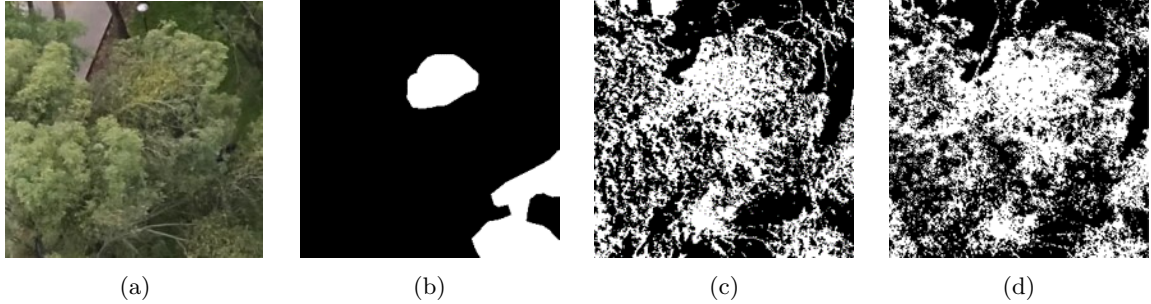


Figure 4: Classification results of *Struthanthus Interruptus*; (a) color image with the presence of mistletoe; (b) mask image; (c) result of experiment 1; (d) result of experiment 5

In addition, hyperparameters were determined using as inputs, all the 180 texture and spectral features, and the spectral bands in combination with the 180 features. Hence, for these two experiments the following values were determined:  $C = 10$  and  $\gamma = 0.001$ . Table 5 presents the classification results, including the Overall Accuracy (OA), Precision (P), Recall (R), and F1-score (F1), obtained by support vector machines trained with the three previously mentioned sets.

The results of these first experiments demonstrated that no matter which set of features is selected for training, the algorithm obtained low precision and regular accuracy and recall values for *S. Interruptus* classification. There is no significant difference between the results of experiments 1 to 3; i.e., since their variation is in the order of hundredths, their performances can be considered as very similar. However, by taking into account the large computational cost involved in calculating the texture features, we can say that it is better to use only the spectral information of the five bands for the current task. Fig 4 shows some classification results of *S. Interruptus* for experiments 1 and 5, respectively.

Table 5: Assessment of classification results using an SVM with a Radial Basis Function, with optimized  $C$  and  $\gamma$  values.

Experiment	Model	OA	P	R	F1
1	5 Bands	0.572	0.258	0.608	0.363
2	180 Features	0.6	0.27	0.584	0.37
3	5 Bands + 180 Features	0.604	0.271	0.574	0.368
4	Bands + Features + PCA	0.581	0.26	0.591	0.361
5	Bands + Features + GA	0.588	0.254	0.590	0.355

### 3.1.1 Feature selection results

In a second stage, we performed two experiments oriented to improve the SVM classification performance by including feature selection processes based on PCA and GA, respectively. PCA has been recognized as a transformation method aimed at dimensional reduction from large data sets; in this transformation, new orthogonal variables maximizing the variance of the input set are determined, which are known as components. Thus, the number of significant components is much lower than the dimensionality of the input set. Hence, PCA has been the basis to select a subset of features.<sup>46,47</sup> On the other hand, the Genetic Algorithms are based on a meta-heuristic inspired by natural selection and inheritance, which are the main forces involved in Darwin's evolution theory, and is usually used for optimization or search problems. GA has been widely used to solve the feature selection problem with promising results.<sup>48,49</sup> For this reason, we explored its use to find a subset of features that maximizes the accuracy in our application.

The SVM classification results using feature selection algorithms can be observed in the last two rows of Table 5. Notice that the GA experiment was executed 30 times. Since the accuracy metrics are similar to the previous experiments, these results suggest that no matter which subset of features we select, the performance of the SVM classifier does not improve significantly. For example, the contributions of descriptors selected by PCA

ranges from -0.1222 to 0.0004, meaning that there is no significant contribution of any feature for classification purposes.

For the GA experiment, each individual was represented by a binary vector, where each element indicates if the corresponding texture feature is used (one), or not (zero), for classification. Then, each individual in the population was evaluated using the selected characteristics, an SVM, and a set of training; the F1 accuracy measure was used to assess the fitness of the individuals. Thus, the GA experiment involved a learning process aimed at improving the average fitness of the initial randomly generated populations. As can be observed in the plot shown in Fig. 5, the fitness value increased from 0.34 to 0.39, at the final generation. Although the fitness improvement resulted in a small value, it suggests that there are subsets of features slightly better than others. Hence, we analyzed the frequency of use of the characteristics of the resulting 30 individuals with the best fitness (one individual by run).

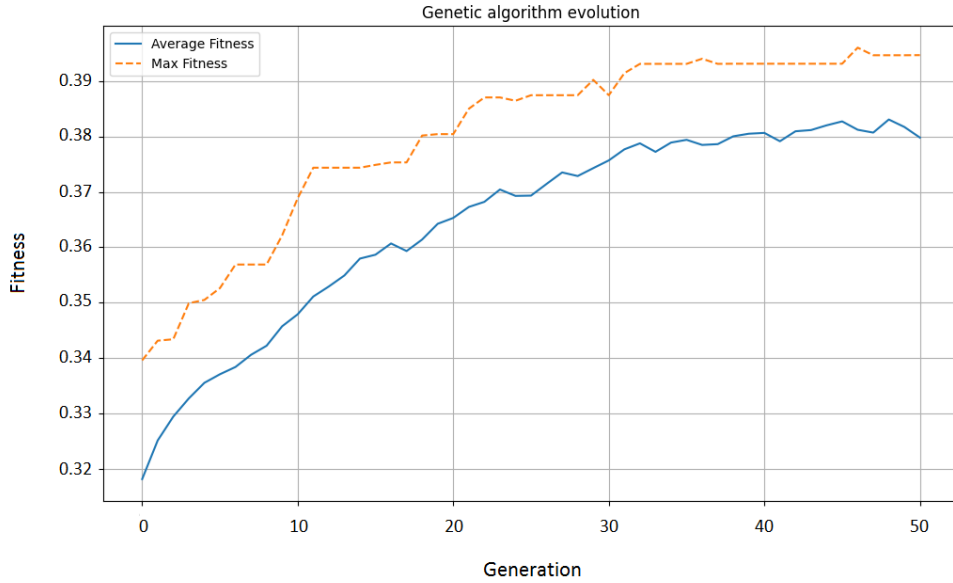


Figure 5: Evolution of GA population fitness through 50 generations.

In general, 76 of the total features were selected by at least 15 of the best individuals. Although the five multispectral bands were not selected, spectral information in the form of vegetation indices was used, as shown in Table 6; additional features that were included in the best individuals are: LBPs computed from bands  $G$  ( $P = 16$  and  $R = 1$ ) and  $REG$  ( $P = 16$  and  $R = 3$ ), respectively.

Table 6: Frequency of use of vegetation indices in the GA experiment.

VI	No	VI	No	VI	No
ARVI	29	GLI	23	GNDVI	20
MSAVI	29	MTVI	23	SAVI	20
MSR	25	SR	22	DVI	19
NDVI	24	RG	22	EVI	19
RDVI	24	CI	20	VARI	19

#### 4. DISCUSSION AND CONCLUSION

Throughout this manuscript, we have performed several experiments oriented to mistletoe classification from aerial multispectral images, collected over an urban park of Mexico City. For this task, we designed five clas-

sification schemes based on a support vector machine, with optimized hyperparameters; motivated by previous researches showing that the performance of machine learning algorithms can be considerably improved by incorporating texture descriptors, we computed a set of 180 image features from the collected imagery, including: gray-level co-occurrence matrix features, Gabor filters, local binary based descriptors, and spectral vegetation indices.

From the augmented image database, different input image sets were employed for training and validation of classification schemes, such as, the spectral bands, texture and spectral features, spectral bands in conjunction with image features, and optimal feature sets determined by either PCA or GA, respectively. The classification results obtained via an SVM algorithm stated that the minimum overall accuracy was obtained when only the five multispectral bands were used as inputs; the accuracy slightly increased when we included the 180 image features in the classification stage. Nevertheless, for this particular application, the use of feature selection techniques did not increase significantly the accuracy metrics, other than one hundredth of magnitude respect to the first experiment. Therefore, we can conclude that no matter which subset of image feature the algorithm selects, the performance of the classifier does not seem to improve.

The aforementioned low results can be related to the similar color and appearance of *S. Interruptus* respect to the host trees, which makes its identification a challenging task, even for a trained expert. Since texture descriptors were defined to capture the intensity variations among neighboring pixels of a given image, while spectral vegetation indices were designed to determine biophysical phenomena of plants, we assumed that their calculus from our image database could increasing the separability between classes (mistletoe/others). However, our results showed that the selected set of features did not contribute significantly to improve the classification performance, being necessary to develop new image features for the current application.

Further research is necessary to advance the classification performance of this particular mistletoe species, which will be oriented in the following directions. Other image acquisition strategies should be considered in order to enhance the visual characteristics of *S. Interruptus*; e.g., by flying the UAV at a lower altitude would increment the spatial resolution of the imagery; image registration over the study area should be realized in a winter season, in which the host trees lose their foliage; a spectral characterization of mistletoe could be necessary to determine spectral regions that increase its visual identification respect to the host trees; additional characteristics of the species could be obtained by a subset of images captured from the basis of the host trees.

Respect to the image processing and classification algorithms, several improvements could be realized on the basis of the actual image database; e.g., by exploring more recent image features and color transformations, we could add a more complete description of the *S. Interruptus* species; because of the use of deep learning techniques, such as Convolutional Neural Networks (CNNs) have demonstrated a high performance for vegetation species classification, their implementation to deal with the current problem on mistletoe classification would be of great interest for the RS community.

## REFERENCES

- [1] Duarte, A., Borralho, N., Cabral, P., and Caetano, M., “Recent advances in forest inspect pests and diseases monitoring using uav-based data: a systematic review,” *Forests* **13**(6) (2022).
- [2] Arriola-Padilla, V. J. et al., “Los muérdagos verdaderos del arbolado de la ciudad de México,” *Revista Mexicana de Ciencias Forestales* **4**(19) (2013).
- [3] Pernar, R., “Detection of mistletoe in digital colour infrared images of infested fir trees,” *Periodicum biologorum* **109**(1), 67–75 (2007).
- [4] Sabrina, F. et al., “Use of deep learning approach on uav imagery to detect mistletoe infestation,” in [IEEE Region 10 Symposium], 556–559 (2020).
- [5] León-Bañuelos, L. et al., “Identification of arceuthobium globosum using unmanned aerial vehicle images in a high mountain forest of central Mexico,” *Journal of Forestry Research* **31**(5), 1759–1771 (2020).
- [6] Miraki, M., Sohrabi, H., Fatehi, P., and Kneubuehler, M., “Detection of mistletoe infected trees using uav high spatial resolution images,” *Journal of Plant Diseases and Protection* **128**, 1679–1689 (2021).
- [7] Mejia-Zuluaga, P. A., Dozal, L., and Valdiviezo-N., J. C., “Genetic programming approach for the detection of mistletoe based on uav multispectral imagery in the conservation area of Mexico city,” *Remote Sensing* **14**(3) (2022).

- [8] Li, Z., Hayward, R., Zhang, J., Jin, H., and Walker, R., “Evaluation of spectral and texture features for object-based vegetation species classification using support vector machines,” *International Archives of the Photogrammetry, Remote Sensing and Spatial Information Sciences - ISPRS Archives* **38** (01 2010).
- [9] Coronado, A. and Moctezuma, D., “Feature evaluation for land use and land cover classification based on statistical, textural and shape features over landsat and sentinel imagery,” *Journal of Applied Remote Sensing* **14**(4), 048503 (2020).
- [10] Muñoz Gutiérrez, L., Pérez Miranda, R., Reséndiz Martínez, J. F., and Reyes Robles, R., “Caracterización de árboles de riesgo en el parque nacional viveros de coyoacán, ciudad de méxico,” *Revista mexicana de ciencias forestales* **13**(72), 201–222 (2022).
- [11] Cibrián Tovar, D., “Diagnóstico fitosanitario de áreas verdes infestadas por muérdago en la Ciudad de México,” (2016).
- [12] Tovar, C., Rosales, A., Díaz, G., Edith, S., et al., “Enfermedades forestales en méxico,” (2007).
- [13] Jensen, J., “Remote sensing of the environment: an earth resource perspective (p. 608),” (2006).
- [14] Myneni, R. B., Hall, F. G., Sellers, P. J., and Marshak, A. L., “The interpretation of spectral vegetation indexes,” *IEEE Transactions on Geoscience and Remote Sensing* **33**(2), 481–486 (1995).
- [15] Huang, S., Tang, L., Hupy, J. P., Wang, Y., and Shao, G., “A commentary review on the use of normalized difference vegetation index (ndvi) in the era of popular remote sensing,” *Journal of Forestry Research* **32**(1), 1–6 (2021).
- [16] Sellers, P. J., “Canopy reflectance, photosynthesis and transpiration,” *International Journal of Remote Sensing* **6**(8), 1335–1372 (1985).
- [17] “Overview of the radiometric and biophysical performance of the modis vegetation indices,” *Remote Sensing of Environment* **83**(1), 195–213 (2002). The Moderate Resolution Imaging Spectroradiometer (MODIS): a new generation of Land Surface Monitoring.
- [18] Huete, A., “A soil-adjusted vegetation index (savi),” *Remote Sensing of Environment* **25**(3), 295–309 (1988).
- [19] Qi, J., Chehbouni, A., Huete, A., Kerr, Y., and Sorooshian, S., “A modified soil adjusted vegetation index,” *Remote Sensing of Environment* **48**(2), 119–126 (1994).
- [20] Kaufman, Y. J. and Tanré, D., “Strategy for direct and indirect methods for correcting the aerosol effect on remote sensing: From avhrr to eos-modis,” *Remote Sensing of Environment* **55**(1), 65–79 (1996).
- [21] Richardson, A. J., Wiegand, C., et al., “Distinguishing vegetation from soil background information,” *Photogrammetric engineering and remote sensing* **43**(12), 1541–1552 (1977).
- [22] Gitelson, A. A. and Merzlyak, M. N., “Remote estimation of chlorophyll content in higher plant leaves,” *International journal of remote sensing* **18**(12), 2691–2697 (1997).
- [23] Barnes, E., Clarke, T., Richards, S., Colaizzi, P., Haberland, J., Kostrzewski, M., Waller, P., Choi, C., Riley, E., Thompson, T., et al., “Coincident detection of crop water stress, nitrogen status and canopy density using ground based multispectral data,” in [*Proceedings of the fifth international conference on precision agriculture, Bloomington, MN, USA*], **1619**, 6 (2000).
- [24] Gitelson, A., Viña, A., Arkebauer, T., Rundquist, D., Keydan, G., Leavitt, B., and Keydan, G., “Remote estimation of leaf area index and green leaf biomass in maize canopies,” *Geophysical Research Letters - GEOPHYS RES LETT* **30** (03 2003).
- [25] Penuelas, J., Baret, F., and Filella, I., “Semi-empirical indices to assess carotenoids/chlorophyll a ratio from leaf spectral reflectance,” *Photosynthetica* **31**(2), 221–230 (1995).
- [26] Haboudane, D., Miller, J. R., Pattey, E., Zarco-Tejada, P. J., and Strachan, I. B., “Hyperspectral vegetation indices and novel algorithms for predicting green lai of crop canopies: Modeling and validation in the context of precision agriculture,” *Remote Sensing of Environment* **90**(3), 337–352 (2004).
- [27] Hussain, S., Gao, K., Din, M., Gao, Y., Shi, Z., and Wang, S., “Assessment of uav-onboard multispectral sensor for non-destructive site-specific rapeseed crop phenotype variable at different phenological stages and resolutions,” *Remote Sensing* **12**(3) (2020).
- [28] Gitelson, A. A., Kaufman, Y. J., and Merzlyak, M. N., “Use of a green channel in remote sensing of global vegetation from eos-modis,” *Remote sensing of Environment* **58**(3), 289–298 (1996).

- [29] Barzin, R., Pathak, R., Lotfi, H., Varco, J., and Bora, G. C., "Use of uas multispectral imagery at different physiological stages for yield prediction and input resource optimization in corn," *Remote Sensing* **12**(15) (2020).
- [30] Gitelson, A. A., Kaufman, Y. J., Stark, R., and Rundquist, D., "Novel algorithms for remote estimation of vegetation fraction," *Remote Sensing of Environment* **80**(1), 76–87 (2002).
- [31] Zhu, G., Ju, W., Chen, J. M., Zhou, Y., Li, X., and Xu, X., "Comparison of forest leaf area index retrieval based on simple ratio and reduced simple ratio," in [2010 18th International Conference on Geoinformatics], 1–4 (2010).
- [32] Gamon, J. and Surfus, J., "Assessing leaf pigment content and activity with a reflectometer," *New Phytologist* **143**(1), 105 – 117 (1999). Cited by: 736.
- [33] Cheng, C., Wei, Y., Lv, G., and Yuan, Z., "Remote estimation of chlorophyll-a concentration in turbid water using a spectral index: a case study in taihu lake, china," *Journal of Applied Remote Sensing* **7**(1), 073465–073465 (2013).
- [34] Roujean, J.-L. and Breon, F.-M., "Estimating par absorbed by vegetation from bidirectional reflectance measurements," *Remote Sensing of Environment* **51**(3), 375–384 (1995).
- [35] Hunt Jr, E. R., Daughtry, C., Eitel, J. U., and Long, D. S., "Remote sensing leaf chlorophyll content using a visible band index," *Agronomy journal* **103**(4), 1090–1099 (2011).
- [36] Chen, J. M. and Cihlar, J., "Retrieving leaf area index of boreal conifer forests using landsat tm images," *Remote sensing of Environment* **55**(2), 153–162 (1996).
- [37] Merzlyak, M. N., Gitelson, A. A., Chivkunova, O. B., and Rakitin, V. Y., "Non-destructive optical detection of pigment changes during leaf senescence and fruit ripening," *Physiologia plantarum* **106**(1), 135–141 (1999).
- [38] Haralick, R., Shannugam, K., Dinstein, I., and Caetano, M., "Textural features for image classification," *IEEE Transactions on Systems, Man, and Cybernetics SMC* **3**(6), 610–621 (1973).
- [39] Mehrotra, R., Namuduri, K., and Ranganathan, N., "Gabor filter-based edge detection," *Pattern Recognition* **25**(12), 1479–1494 (1992).
- [40] Rabatel, G., Delenne, C., and Deshayes, M., "A non-supervised approach using gabor filters for vine-plot detection in aerial images," *Computers and Electronics in Agriculture* **62**(2), 159–168 (2008).
- [41] Brenning, A., Long, S., and Fieguth, P., "Detecting rock glacier flow structures using gabor filters and ikonos imagery," *Remote Sensing of Environment* **125**, 227–237 (2012).
- [42] Chen, Y., Zhu, L., Ghamisi, P., Jia, X., Li, G., and Tang, L., "Hyperspectral images classification with gabor filtering and convolutional neural network," *IEEE Geoscience and Remote Sensing Letters* **14**(12), 2355–2359 (2017).
- [43] Jumarie, G., "Entropy of markovian processes: Application to image entropy in computer vision," *Journal of the Franklin Institute* **335**(7), 1327–1338 (1998).
- [44] Ojala, T., Pietikainen, M., and Maenpaa, T., "Multiresolution gray-scale and rotation invariant texture classification with local binary patterns," *IEEE Transactions on Pattern Analysis and Machine Intelligence* **24**(7), 971–987 (2002).
- [45] Divakar, M. S., Elayidom, M. S., and Rajesh, R., "Analysis of remote sensing satellite imagery for crop yield mapping using machine learning techniques," in [Congress on Intelligent Systems: Proceedings of CIS 2021, Volume 1], 689–700, Springer (2022).
- [46] Song, F., Guo, Z., and Mei, D., "Feature selection using principal component analysis," in [International Conference on System Science, Engineering Design and Manufacturing Informatization], IEEE (2010).
- [47] Odhiambo-Omuya, E., Onyango-Okeyo, G., and Waema, K., "Feature selection for classification using principal component analysis and information gain," *Expert Systems with Applications* **174**(114765) (2021).
- [48] Siedlecki, W. and Sklansky, J., "A note on genetic algorithms for large-scale feature selection," *Pattern Recognition Letters* **10**(5), 335–347 (1989).
- [49] Sohail, A., "Genetic algorithms in the fields of artificial intelligence and data science," *Annals of Data Science* **10**, 1007–1018 (2021).